23rd International Conference on Material Forming (ESAFORM 2020)

Process-oriented Flow Curve Determination at Mechanical joining

M. Jäckel[a*], S. Coppieters[b], N. Vandermeiren[c],

C. Kraus[a], W.-G. Drossel[a], N. Miyake[d], T. Kuwabara[d], K. Unruh[e], T. Balan[f], H. Traphöner[g] and A. E. Tekkaya[g]

[a]*Fraunhofer Institute for Machine Tools and Forming Technology IWU, Nöthnitzer Straße 44, Dresden 01187, Germany*
[b]*KU Leuven, Technology Campus Ghent, Department of Materials Engineering, Gebroeders De Smetstraat 1, Ghent 9000, Belgium*
[c]*Belgium Welding Institute, Technologiepark 48, Ghent 9052, Belgium*
[d]*Institute of Engineering, Tokyo University of Agriculture and Technology, 3 Chome-8-1 Harumicho Tokyo 183-8538, Japan*
[e]*Faurecia Autositze GmbH, Nordsehler Straße 38, Stadthagen 31655, Germany*
[f]*Université de Lorraine, Arts et Métiers ParisTech, LCFC, Metz F-57000, France*
[g]*Institute of Forming Technology and Lightweight Components, TU Dortmund, Baroper Straße 303, Dortmund 44227, Germany*

* Corresponding author. Tel.: +32 (0)9 292 14 25; fax: +32 (0)9 292 14 01. *E-mail address:* nelis.vandermeiren@bil-ibs.be

Abstract

The accuracy of numerical simulation models for forming processes depends highly on the method for the flow curve determination. Numerous experimental tests exist to identify the flow curves of sheet metals, each with certain characteristics regarding stress states and achievable strains. In this paper stress state analysis are presented for the mechanical joining techniques clinching as well as self-pierce riveting with semi-tubular rivet (SPR). Based on these findings flow curves for DC04 material are determined by selected experimental materials tests in order to compare the influence of the flow curve determination method on the accuracy of the process simulation models.

1. Introduction

The predictive accuracy of finite element simulations for forming and joining by forming of sheet metal largely depends on the adopted material model. Many of these processes generate severe plastic deformation of the sheet metal. For example, during joining by forming of sheet metal (e.g. clinching) a multitude of stress states are generated accompanied with large plastic straining of the material. From a simulation point of view, however, plastic anisotropy of the sheet metal can be safely ignored for predicting the metal flow [1]. Indeed, the metal flow is strongly constrained by the joining tools preventing plastic anisotropy to manifest itself at the length scale of the joint. As such, joining by forming is usually simulated assuming a von Mises material solely requiring a large strain flow curve to account for strain hardening. Obviously, standard tensile tests are of limited usefulness because necking limits uniform deformation. Several experimental techniques have been developed [2,3,4,5,6] determine the large strain flow curve of sheet

metal. In this regard, there are two issues. Firstly, these material tests are typically dominated by a certain stress state and yield different results depending on the degree of plastic anisotropy. Secondly, due to the small dimensions of the forming tools (e.g. punch or rivet) compared to the nominal sheet thickness, joining by forming processes of sheet metal must be regarded as a bulk forming problem in which the through-thickness stress cannot be ignored. The crux of the problem here is that the plastic material behavior of sheet metal is conventionally determined using material tests, which are confined to homogeneous plane stress conditions in the plane of the sheet.

Sheet metal itself often exhibits plastic anisotropy. As such, when adopting the von Mises criterion for simulating joining by forming, it is crucial to identify the flow curve using a material test, which generates a stress state resembling the dominating stress state during the joining process. The aim of this paper is to present a generic methodology to identify the dominating stress state in joining by forming processes, which can be used to select the most appropriate material test to identify the large strain flow curve.

2. Considered joining by forming technologies

2.1. Clinching

Clinch forming allows assembling thin metal parts by solely relying on local plastic deformation of the base material. Clinching does not use additional consumables (such as rivets). The basic principle of clinch forming processes is to create an interlock between the combining thin metal parts with the aid of relatively simple tools like a punch, a blank holder and a die (fig. 1). The punch locally pushes metal into the die and, depending on the shape of these clinching tools, the resulting metal flow targets the creation of a mechanical interlock. [7]
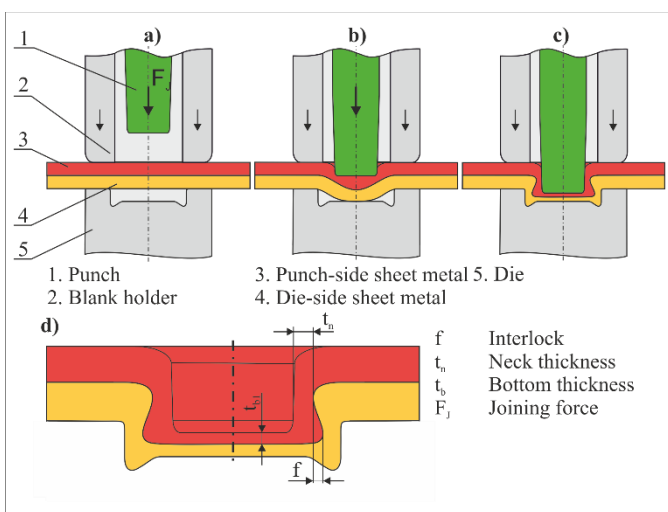

Fig. 1. Clinching: a) – c) Process steps, d) Characteristic values [7]

Clinching joints are evaluated by certain characteristic values like interlock f and neck thickness t_n, which directly correlate with the strength of the joints.

2.2. Self-pierce riveting

In the first process step of self-pierce riveting with semi-tubular rivets (SPR), the parts and the rivet are positioned between punch, blank holder and die (Fig. 2a). Next, the punch presses the semi-tubular rivet into the parts. Due to the cutting edge of the rivet, a slug is punched out of the punch-side part and is enclosed inside the rivet (Fig. 2b). Following, the shape of the die causes the rivet to expand and creates an interlock (Fig. 2c). At the end, the cavity of the die can be completely filled with material [8].
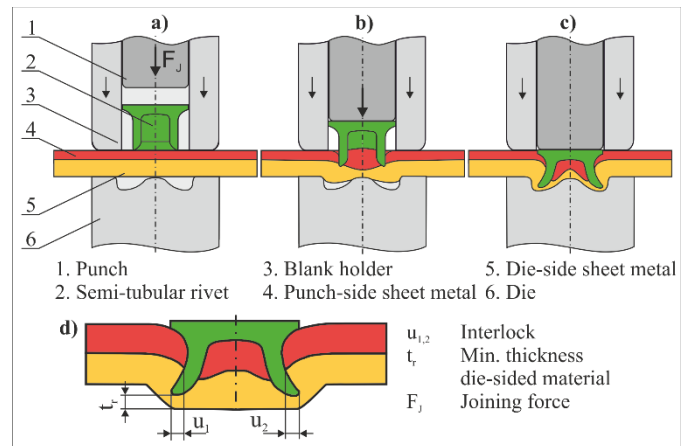

Fig. 2. Self-pierce riveting: a) – c) Process steps, d) Characteristic values [8]

SPR joints are evaluated by certain characteristic values (Fig. 2d) like interlock $u_{1,2}$ and minimal thickness of the die-sided part t_r, which directly correlate with the strength of the joints.

3. Stress state analysis

3.1. Method

If the material exhibits plastic anisotropy, it seems important to calibrate the von Mises yield criterion to a stress state, which dominates the joining process. The latter procedure can be regarded as stress state fitting, and, consequently, selection of a proper material test requires a stress state analysis. Since the deformation is expected to be complex, numerical simulation is used for the stress state analysis. A 3D stress state can be unambiguously described by the Lode angle ξ and the triaxiality η [9].

Fig. 3 shows the (ω-η)-diagram, where the stress metric ω is defined as $\omega = 1-\xi^2$. For shear-dominated stress states ω equals 1, while for axisymmetric stress states ω equals 0. The red curve shown in the (ω-η)-diagram is the so-called plane stress path directly derived from the plane stress von Mises yield locus. The area which deviates from the plane stress path is subjected to a 3D stress state. Following the considered joining technologies as well as the material tests will be evaluated regarding their stress state using this method.
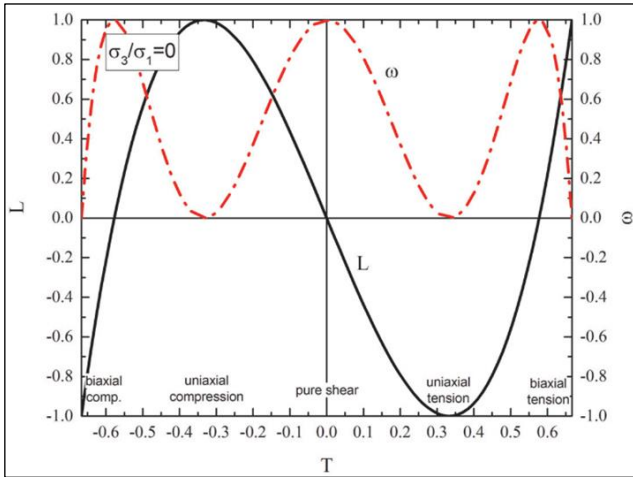
Fig. 3. Stress-state analysis: the (ω-η)-diagram. [10]

3.2. Clinching

Fig. 4a) shows the calculated strains, instantanous triaxiality 4b) and the instantanous stress metric ω 4c) at the end of the clinching process of DC04 ($t = 1.0$ mm) in DC04 ($t = 1.0$ mm). The largest strains of approximately 2 occur in the region of the interlock. It can be inferred that at the end of joining process, the bottom of the joint is dominated by pure compressive stresse state ($\omega = 0$, $\eta < 0$) .
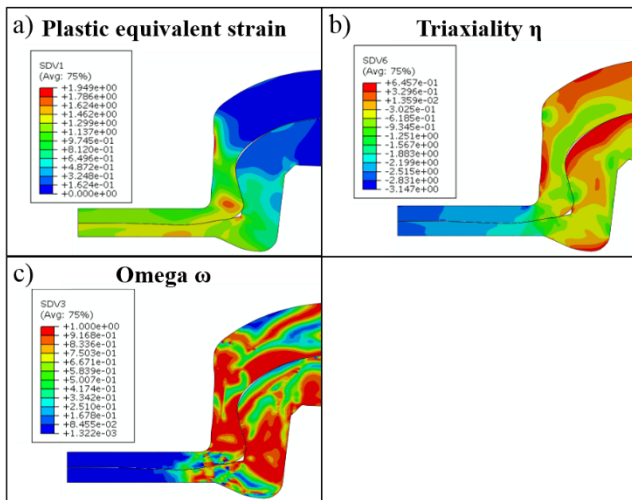

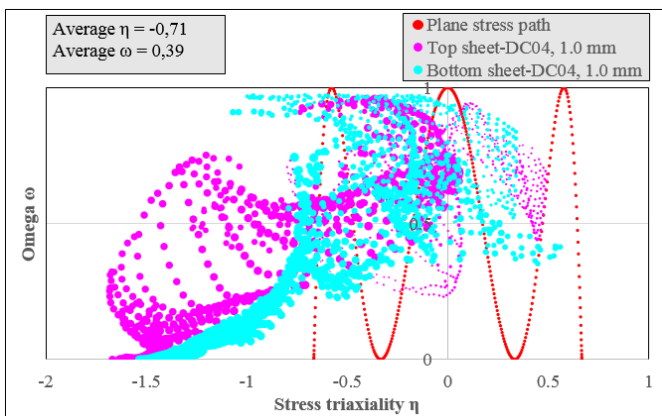Fig. 4. Process simulation Clinching: a) Plastic equivalent strain b) Triaxiality c) Stress metric ω

Fig. 5. ω-η-diagram for Clinching of DC04 in DC04

The necking region is shear-dominated while in the transiation towards the bottom a diverse stress state prevails. Fig. 5 simultaneously visualizes the averaged values of ω and η of each of the platically deforming finite elements in the (ω-η)-diagram. Thereby the size of the bubbles corresponds to the magnitude of the equivalent plastic strain in the considered material point of the top and bottom sheet. It can be seen that the stress and strain state of the upper and lower sheet is comparable. The large plastic deformation is predominantly associated with negative triaxixlity. The occuring shear stresses are relativly diverse with an average of all considered elements of $\omega = 0.39$. However, by binning ω and analyzing the consumed plastic work it can be shown [11] that 20 % of plastic work is associated with $0 \leq \omega \leq 0.1$ and $\eta < 0$. As such, the SCT seems to be a good choice for the identification of the flow curve.

3.3. Self-pierce riveting (SPR)

Fig. 6 visualizes the strain and stress condition for SPR of the same material combination as for clinching. At the end of the SPR process even larger, local strains occur of approximately 3.8. Thereby, especially the region below the rivet, a high hydrostatic pressure arises with triaxiality between $-1 \leq \eta \leq -4$.
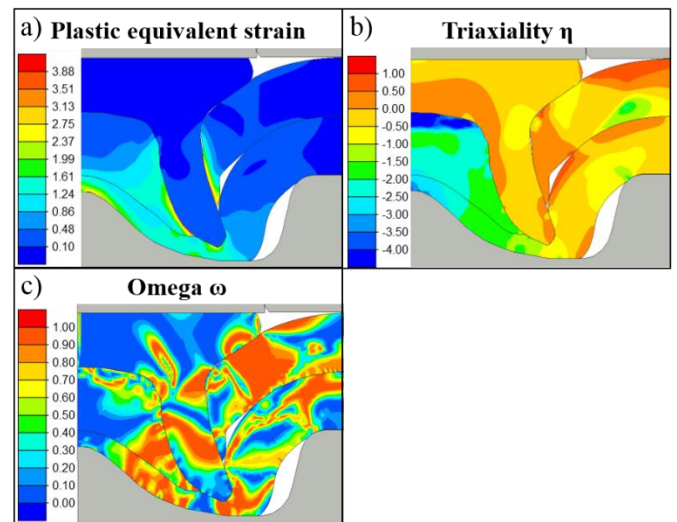

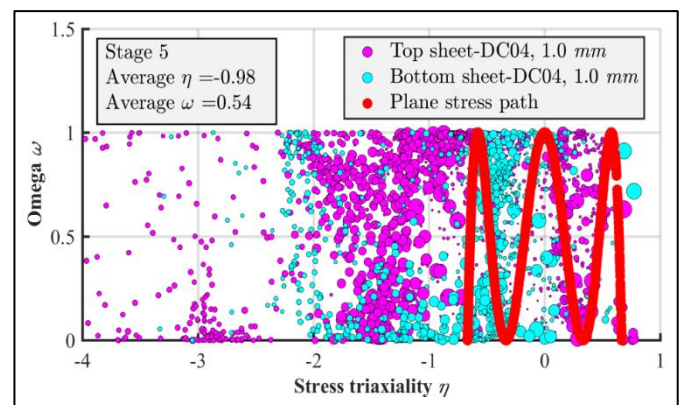Fig. 6. Process simulation SPR: a) Plastic equivalent strain b) Triaxiality c) Stress metric ω

Fig. 7. ω-η-diagram for SPR of DC04 in DC04

In regards to shear stresses the results SPR for both the top and bottom sheet are very diverse (Fig. 7) with an average value similar to clinching of $\omega = 0.54$.

4. Flow curve determination methods

In this section, five material tests are used to determine the large strain flow curve of DC04 sheet with a nominal thickness of 1 mm and an average r-value of $r_{avg} = 1.64$. All these test represent a certain stress state (Fig. 8).
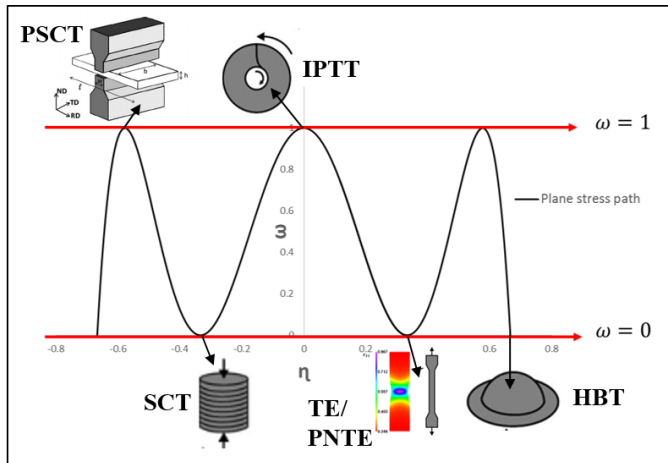

Fig. 8. Classification of the considered sheet metal test methods test in the ω-η-diagram

A quasi-static tensile test (TE) in Rolling Direction (RD) was conducted on a standard tensile machine with a load capacity of 10 kN. Additionally, the tensile machine was equipped with a stereo Digital Image Correlation (DIC) system to measure the full-field displacements fields within the diffuse neck during a quasi-static Post-Necking Tensile Experiment (PNTE). The energy method was used to inversely identify the post-necking hardening parameter p [2] using 121 load steps. The dashed red curve shown in Fig. 8 is the resulting PNTE-flow curve. It has been shown that the energy method [1] extends the validity of the standard tensile test and generally enhances the fitting quality of phenomenological hardening laws in the post-necking regime.

The Stack Compression Test (SCT) [3] was carried out on a electro-mechanical press with a maximum press force of 100 kN using 3 disks. Lubrication was applied to minimize the effect of friction. The green line in Fig. 1 shows the experimentally acquired flow curve using the SCT.

The hydraulic bulge test (HBT) [4] enables to probe large plastic strains under quasi-balanced biaxial tension. The thickness plastic strain ε_z^p and the radius of curvature ρ at the top of the bulged specimen were measured using a stereo DIC system. The orange curve in Fig. 1 shows the flow curve measured using the strain-controlled HBT.

The setup for in-plane torsion test (IPTT) [5] consists of an inner clamp and an outer clamp and the circular specimen, which is fixed between these clamps. The measurement of torque is done by a static torque sensor attached to the outer clamp of the torsion device. The inner clamping force F of 100 kN is applied by a Zwick 100 kN universal testing machine and a servo motor with two gears drives the outer clamp at $r = 30$ mm with a rotational speed of 3.3 °/min during the experiment. The inner clamp at $r = 15$ mm is kept fixed. This imparts shear stress state in the sheet which varies in gradient along the radial direction with maximum value at the inner clamp radius. Trough the IPTT strains (Fig. 9, purple line) up to 1.2 were conducted.

At the plane strain compression test [6] the sheet metal strip is pressed between the upper and lower tools forming an indentation in the middle. The friction in the contact region is mimimizedby applying a layer of grease and teflon on both surfaces of the specimen. The resulting flow curve is represented by the yellow line in Fig. 9.
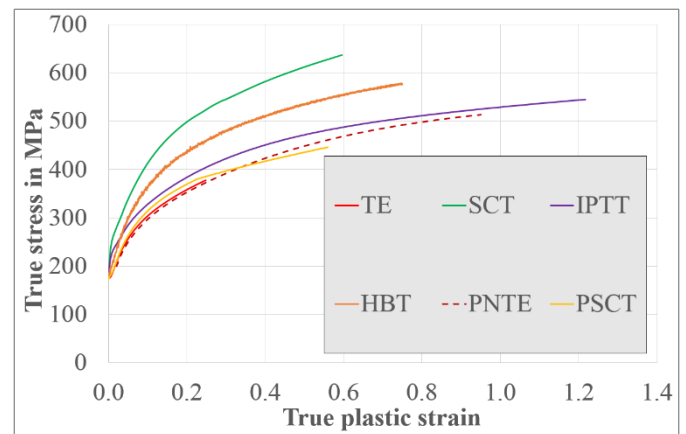

Fig. 9. Flow curves for DC04 determined with the considered material tests

From Fig. 9 it can be seen that initial yielding corresponds to a von Mises material. Beyond initial yielding, however, the flow curve strongly depends on the adopted material test indicating the occurrence of differential work hardening, which is a typical observation for low carbon steel sheet with an average r-value $r_{avg} > 1.5$ [12]. From the equivalence of work hardening in terms of plastic work it can be shown that the HBT-flow curve can be converted to an uniaxial stress-plastic strain curve in the RD [4]. The concept of work conjugate shows that the converted HBT-flow curve correspondence with the PNTE-flow curve. The latter is recently also observed by Hakoyama et al. [13]. As such, it can be stated that the post-necking strain hardening rate identified by the HBT and the PNTE is in good agreement. Moreover, it can be inferred from Fig. 9 that the IPTT yields a post-necking strain hardening behaviour that is in good agreement with the PNTE. The IPTT enables to probe the largest plastic equivalent strain (approximately 1.2).

The most remarkable observation in the post-necking regime is that the SCT-flow curve exhibits significantly more strain hardening than observed in the other experiments. In terms of stress state, the SCT is equivalent to the HBT assuming that hydrostatic pressure does not affect plastic yielding. As such, the discrepancy between the flow curves obtained through the HBT and the SCT suggests that the hydrostatic stress component affects the flow stress.

5. Numerical assessment of flow curves

5.1. Clinching

At the numerical assessment the determined flow curves from the considered material tests were implemented in the simulation model of the clinching process and are compared to the experimental results. Since the occuring strains at the clinching and SPR process exceed the strains determined from the material tests the flow curves used in the following numerical assessment were extrapolated using the Swift model [14].

Fig. 10 shows the metal flow a), the process force-displacement graph b) as well as the chracteristic values c) for the experiment and calculated results. In terms of metal flow (Fig. 10a) only minor differences can be observed. All simulations with the different flow curves are in good agreement with the experiment. When comparing the characteristic values (Fig. 10c) interlock f and neck thickness t_n , the process simualtion with the SCT flow curve delivers the lowest difference to the experiment.

c)

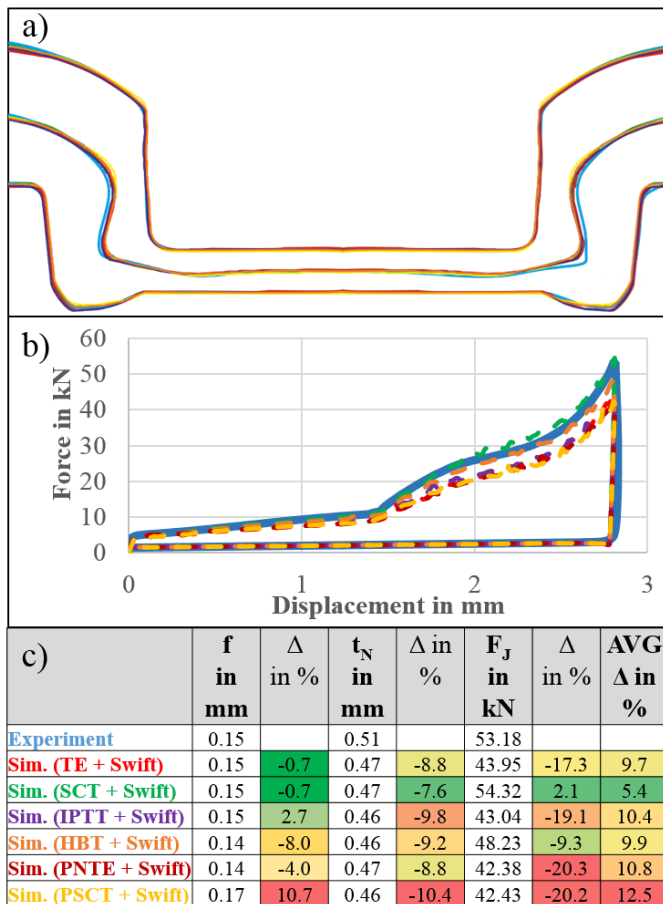|	f in mm	Δ in %	t_N in mm	Δ in %	F_J in kN	Δ in %	AVG Δ in %
Experiment	0.15		0.51		53.18		
Sim. (TE + Swift)	0.15	-0.7	0.47	-8.8	43.95	-17.3	9.7
Sim. (SCT + Swift)	0.15	-0.7	0.47	-7.6	54.32	2.1	5.4
Sim. (IPTT + Swift)	0.15	2.7	0.46	-9.8	43.04	-19.1	10.4
Sim. (HBT + Swift)	0.14	-8.0	0.46	-9.2	48.23	-9.3	9.9
Sim. (PNTE + Swift)	0.14	-4.0	0.47	-8.8	42.38	-20.3	10.8
Sim. (PSCT + Swift)	0.17	10.7	0.46	-10.4	42.43	-20.2	12.5

Fig. 10. Comparison of simulation results with different flow curves for Clinching of DC04 in DC04: a) joint formation b) Force displacement diagram c) Characteristic joint values

More significant disparities can be seen in the comparison of the course of the process forces. Especially towards the end of the clinching process the experiment can be modelled better by the simulation model with the flow curve form SCT and HBT. It must be noted that the process graph enables to

indirectly assess predictive accuracy of the FE model with respect to the stress levels within the joint. The latter becomes relevant when embarking on performance simulations to assess the strength of the joint.

5.2. Self-pierce riveting

When comparing the calculated joining contours with the experiment for SPR (Fig.11a), larger differences can be observed than for clinching. It can be observed that the flow curves of the parts to be joined have a significant influence on the rivet spreading. The rivet spreading is best represented by the process simulation with the SCT flow curve, which also shows the least significant deviations from the experiment with respect to the geometrical characteristics interlock $u_{1,2}$ and especially the minimum thickness of the die-side material t_r (Fig. 11c).

c)

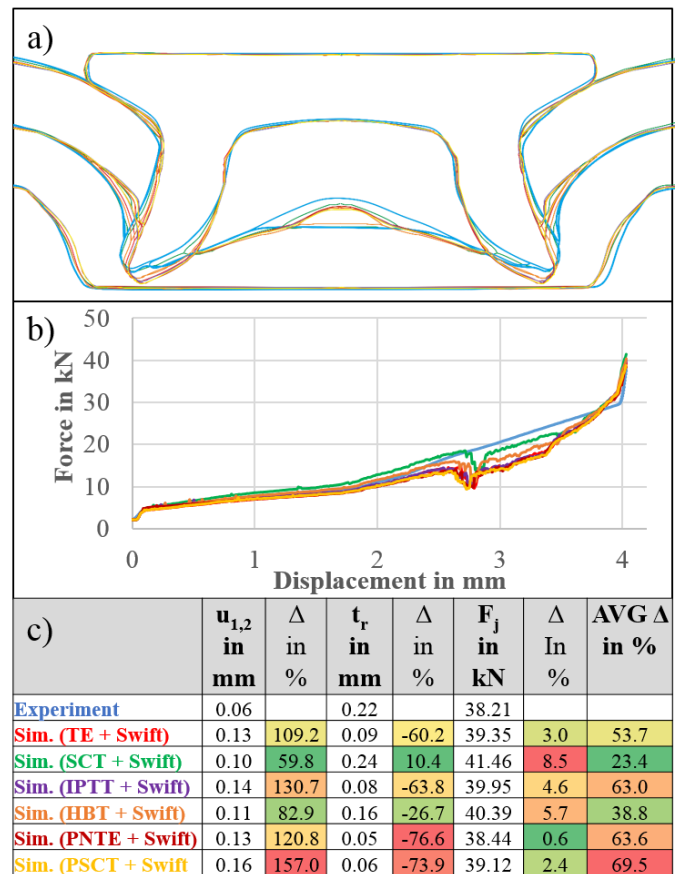|	$u_{1,2}$ in mm	Δ in %	t_r in mm	Δ in %	F_j in kN	Δ In %	AVG Δ in %
Experiment	0.06		0.22		38.21		
Sim. (TE + Swift)	0.13	109.2	0.09	-60.2	39.35	3.0	53.7
Sim. (SCT + Swift)	0.10	59.8	0.24	10.4	41.46	8.5	23.4
Sim. (IPTT + Swift)	0.14	130.7	0.08	-63.8	39.95	4.6	63.0
Sim. (HBT + Swift)	0.11	82.9	0.16	-26.7	40.39	5.7	38.8
Sim. (PNTE + Swift)	0.13	120.8	0.05	-76.6	38.44	0.6	63.6
Sim. (PSCT + Swift)	0.16	157.0	0.06	-73.9	39.12	2.4	69.5

Fig. 11. Comparison of simulation results with different flow curves for SPR of DC04 in DC04: a) joint formation b) Force displacement diagram c) Characteristic joint values

In regard to the course of the process forces differences also become apparent in the second half of the process. The drop in joining force at a distance of approx. 2.8 is, however, due to the deletion of elements, which cannot currently be avoided for material separation in SPR.

6. Conclusion

This paper deals with the exploration of a process-informed methodology for selecting the most appropriate material test for identifying the large strain flow curve of sheet metal.

For an anisotropic material like DC04 the flow curves from the considered material tests vary signifiantly due to the different stress conditions of the material tests. In addition, it can be stated that the maximum achievable strain varies significantly depending on the adopted material test. In the investigations described here, the largest strain for DC04 of approx. 1.2 was achieved by the in-plane torsion test.

The selection procedure relies on a first order simulation for feeding the stress state analysis. The basic idea is to identify the dominating stress state in joining process. This information along with the average plastic strain is linked with the most appropriate material test for identying the large strain flow curve. The methodology is applied and validated to the problem of clinch forming and self-pierce riveting. A comparison of the process simulations of clinching and self-pierce riveting with flow curves from different material tests showed the best comparability to the experiment with the flow curves from the stack compression test. This confirmed the methodology proposed in this paper.

Acknowledgements

References

[1]   Coppieters, S.: *Experimental and numerical study of clinched connection*, PhD thesis, KU Leuven, 2012.

[2]   Coppieters S., Kuwabara T.: *Identification of post-Necking hardening phenomena in ductile sheet metal.* Exp. Mech. 54:1355-1371, 2014.

[3]   Steglich D., Tian X., Bohlen J., Kuwabara T.: *Mechanical testing of thin sheet magnesium alloys in biaxial tension and uniaxial compression.* Exp. Mech. 54:1447-1258, 2014.

[4]   ISO 16808:2014 : *Metallic materials –Sheet and strip – Determination of biaxial stress-strain curve of bulge test with optical measuring systems*

[5]   Traphöner, H., Clausmeyer, T., Tekkaya, A. E.: *Material Characterization for Plane and Curved Sheets Using the In-Plane Torsion Test – An Overview.* Journal of Materials Processing Technology 257, pp. 278-287, 2018.

[6]   Chermette, C., Unruh, K., Peshekhodov, I. et al. Int J Mater Form 2019.

[7]   DVS Gemeinschaftsausschuss „Mechanisches Fügen": *DVS/EFB Merkblatt 3420 Clinchen - Überblick.* DVS-Verlag: Düsseldorf, Germany, 2012.

[8]   DVS Gemeinschaftsausschuss, Mechanisches Fügen. *DVS/EFB Merkblatt 3410 Stanznieten-Überblick.* DVS-Verlag: Düsseldorf, Germany, 2014.

[9]   Bai Y., Wierzbicki, T.: *A new model of metal plasticity and fracture with pressure and Lode dependence.* Int. J. Plas. 24:1071-1096, 2008.

[10]   Testa, G., Ruggiero, A., Iannitti, G., Bonora, N., Gentile, D.: *Modification of the Bonora Damage Model for shear failure*, Frattura ed Integrità Strutturale, 44 (2018) 140-150.

[11]   Coppieters, S., Jäckel, M. et al: *Large Strain Flow Curve Identification for sheet metal: Process informed method selection.* Forming Technology Forum 2019, September 19-20, Hersching am Ammersee, Germany

[12]   Sekiguchi, C., Saito, M., Kuwabara, T.: *Measurement and analysis of the differential work hardening of ultra-low carbon steels.* Key Eng. Mater. 651-653: 552-557, 2015.

[13]   Hakoyama T., Coppieters, S., Kuwabara, T.: *Effect of strain rate on determining post-necking work hardening of a low-carbon sheet steel.* NUMIFORM 2019, June 23-27, New Hampshire, USA.

[14]   Swift, H. W.: *Plastic instability under plane stress.* Journal of the Mechanics and Physics of Solids, 1 (1), 1–18. 195